

International Journal of Modern Physics D
 © World Scientific Publishing Company

Expected coalescence rates of NS-NS binaries for laser beam interferometers

J. A. de Freitas Pacheco¹, T. Regimbau^{2,3}, S. Vincent¹ and A. Spallicci²

¹UMR 6202 Cassiopée, CNRS, Observatoire de la Côte d'Azur, BP 4229, 06304 NICE Cedex 4 (France)

²UMR 6162 Artemis, CNRS, Observatoire de la Côte d'Azur, BP 4229, 06304 NICE Cedex 4 (France)

³School of Physics and Astronomy, Cardiff University, 5 The Parade, Cardiff, CF2 3YB, United Kingdom

pacheco@obs-nice.fr, regimbau@obs-nice.fr, vincent@obs-nice.fr, spallicci@obs-nice.fr

Received Day Month Year

Revised Day Month Year

Communicated by Managing Editor

The coalescence rate of two neutron stars (NS) is revisited. For estimation of the number of bound NS-NS and the probability of their coalescence in a timescale τ , the galactic star formation history, directly derived from observations, and the evolution of massive stars are considered. The newly established galactic merging rate is $(1.7 \pm 1.0) \times 10^{-5} \text{ yr}^{-1}$, while the local merging rate, including the contribution of elliptical galaxies, is about a factor of two higher, $3.4 \times 10^{-5} \text{ yr}^{-1}$. Using the present data basis on galaxy distribution in the local universe and the expected sensitivity of the first generation of laser beam interferometers, we estimate that one event should occur every 125 years for LIGO and one event each 148 years for VIRGO. The situation is considerably improved for advanced-LIGO since we predict that 6 events per year should be detected whereas for a recently proposed VIRGO new configuration, the event rate might increase up to 3 events every two years.

Keywords: gravitational waves; neutron star binaries; laser interferometers

1. Introduction

The merger of two neutron stars (NS-NS), two black holes (BH-BH) or a black hole and a neutron star (BH-NS) are among the most important sources of gravitational waves, due to the huge energy released in the process. In particular, the coalescence of NS-NS binaries may radiate about 10^{53} erg in the last seconds of their inspiral trajectory, at frequencies up to 1.4-1.6 kHz, range covered by most of the ground-based laser interferometers like VIRGO¹, LIGO², GEO³ or TAMA⁴. For understanding of the process dynamics, the prediction of its signal waveform, the estimate of its released power and the event rate, theoretical studies on the coalescence of NS-NS systems have been performed in the past years^{5,6,7}. The dynamics of the inspiral and, in particular, the study of tidal effects in the very last

orbits, may put strong constraints on the equation of state of dense matter. Concerning the coalescence rate of NS-NS binaries, theoretical evaluations are always performed in two main steps: firstly, the merging rate in our Galaxy is estimated and then, assuming that this rate is typical, an estimate is performed for the volume of the universe sampled by a given detector, using some adequate scaling. The galactic merging rate has been estimated either by using binary population synthesis models^{8,9,10} or from the statistics of the observed NS-NS binaries^{11,12,13,14,15}. These estimates may differ by one order of magnitude, ranging in general from 10^{-6} yr^{-1} up to few times 10^{-5} yr^{-1} , but values as high as $\sim 3 \times 10^{-4}$ yr^{-1} have been reported in the literature^{16,17}. Recently Ref. 18 included the new highly relativistic NS-NS binary system PSR J0737-3039 in their statistical analysis, obtaining a value ($\sim 8.3 \times 10^{-5}$ yr^{-1}) comparable to the high rates derived previously by Ref. 16 and Ref. 17. Once the present galactic merging rate has been evaluated, the expected detection rate can be estimated by scaling the total luminosity within the volume probed by the detector with respect to the luminosity of the Galaxy at the same wave-band. Within the local universe ($z < 0.01$), the distribution of galaxies is not homogeneous and if the actual distribution is not taken into account, the expected detection rate may be seriously underestimated¹⁹. For instance, the inclusion of the huge concentration of galaxies in the direction of Norma-Centaurus may considerably increase the detection rate of these events²⁰. Estimates of the galactic merging rate performed according to a given evolutionary model, require the knowledge of the star formation history. These models assume usually that the star formation rate is proportional to the available mass of gas and a consequent exponential decay with time. However, observations and numerical simulations suggest that "disky" galaxies, including the Milky Way, are gradually formed by accretion and merger episodes^{21,22}, which affect the star formation history. It is clear that in spite of all efforts made in the past years to evaluate the local coalescence rate and the expected detection rate by a given interferometric detector, the uncertainties are still quite large with consequences bearing on the future development of instruments and the detection strategy. In the present work, we combine the advantages of different approaches to present a new estimate of galactic merging rate based on population synthesis of the pulsar population^{23,24} and on new simulations on the evolution of massive binaries. From the latter, we have derived the distribution probability $P(\tau)$, which gives the fraction of newly formed NS-NS binaries with a coalescence timescale τ , due to gravitational radiation losses. For the first time the star formation history of our Galaxy, derived directly from observations, was included in the computation of the galactic NS-NS merging rate. Since elliptical galaxies contribute also to the morphological composition of galaxies in the local universe, we have estimated the expected coalescence rate in these objects, by adopting a star formation model able to reproduce their observed photometric properties. Then, the local average coalescence rate has been estimated and weighted according to the total light fraction contribution of each morphological type. In a second step, we evaluate the volume of the universe probed by a given detector and compute the total luminosity

inside this volume, using available data basis. The organization of this paper is the following: in Section II we present the derivation of the local coalescence rate, in Section III we estimate the expected detection rates taking into account the planned sensibility of the different interferometers and, finally, in Section IV we discuss our results and summarize our main conclusions.

2. The local coalescence rate

2.1. The galactic rate

In order to calculate the coalescence rate of NS-NS pairs in a given galaxy, we adopt here the approach by Ref. 20. Let us suppose that a massive binary (masses of components higher than $9 M_{\odot}$) is formed at the instant t' . Let τ_* be the mean evolutionary timescale required for the system to evolve into two neutron stars, typically of the order of $10^7 - 10^8$ yr. Define $P(\tau)$ as the probability per unit of time for a newly formed NS-NS binary to coalesce in a timescale τ and define $R_*(t)$ as the star formation rate, given in $M_{\odot} \cdot \text{yr}^{-1}$. Under these conditions, the coalescence rate at instant t is

$$\nu_c(t) = f_b \beta_{ns} \lambda \int_{\tau_0}^{(t-\tau_*)-\tau_0} P(\tau) R_*(t - \tau_* - \tau) d\tau \quad (1)$$

where f_b is the fraction of massive binaries formed among all stars, β_{ns} is the fraction of formed binaries which remain bounded after the second supernova event and λ is the fraction per unit mass of formed stars in the mass interval $9-40 M_{\odot}$. We assume that progenitors with initial masses above $40 M_{\odot}$ will produce black holes. We have set τ_0 as the minimum timescale for a NS-NS binary to coalesce. This minimum timescale was estimated from simulations to be described below. If the initial mass function (IMF) is of the form $\xi(m) = Am^{-\gamma}$, with $\gamma \approx 2.35$ (Salpeter's law), normalized within the mass interval $0.1 - 80 M_{\odot}$ such as $\int m \xi(m) dm = 1$, then $\lambda = \int_9^{40} 0 \xi(m) dm = 5.72 \times 10^{-3} M_{\odot}^{-1}$. The parameters β_{ns} , τ_0 and the probability distribution $P(\tau)$ were calculated from numerical simulations described in detail by Ref. 25. Here we outline only the main aspects of these simulations. A massive binary is initially generated according to the following prescriptions. The mass of the primary is obtained from a probability distribution corresponding to a Salpeter's IMF, while the secondary mass is derived from the observed mass ratio distribution for massive binaries obtained from observations²⁶. The initial pair separation a is fixed by a probability distribution $P(a) \propto da/a$ ³⁹, normalized between R_{min} and R_{max} . The minimum separation was taken to be equal to twice the Roche lobe of the primary and the maximum separation was taken to be equal to $100R_{min}$. The initial eccentricity of the orbit was assumed to obey a distribution probability $P(e)de = 2ede$, corresponding to orbits filling completely the phase space. Until the explosion of the first supernova (the primary star), the orbital parameters of the system vary due to the mass-loss produced by the stellar wind from both stars or mass transfer. The latter mechanism is more rare, since these massive stars do

not frequently reach or overlap the Roche-lobe. The explosion of the first supernova leaves a NS remnant of $1.4 M_{\odot}$ and produces an "instantaneous" mass loss, which may disrupt (total orbital energy positive after the event) or not (total orbital energy negative after the explosion) the originally bound pair. Our simulations indicate that 77.4% of the systems remain bounded after the first supernova. The bound binary, now constituted by a NS star and an evolved star, which has already lost part of its original mass, enters into a second phase of slow mass-loss, with the orbital parameters varying as before, until the second supernova explosion occurs. We recall that our evolutionary scenario is similar to that developed by Ref. 10, in which none of the stars ever had the chance of being recycled by accretion. We have performed 500,000 numerical experiments, from which resulted 11,627 NS-NS bound pairs, implying $\beta_{ns} = 0.024$. A velocity kick is probably imparted to the nascent neutron star although its mechanism is still a matter of debate. Natal kicks may unbind binaries which otherwise might have remained bound or, less probably, conserve bound systems which without the kick would have been disrupted. In these experiments we have assumed that neutron stars have a natal kick velocity corresponding to a 1-D velocity dispersion of about 80 km/s. We have also investigated how these results are changed if a Maxwellian velocity distribution with a dispersion 1-D of 230 km/s is adopted. In this case, the resulting fraction of bound binaries is reduced by one order of magnitude, e.g., $\beta_{ns} = 0.0029$. These numbers corresponding to the resulting fraction of bound systems are consistent with previous analyses on effects of the natal kick^{17,9}. Recent investigations on the spin period-eccentricity relation for NS-NS systems²⁸ suggest that such a correlation can only be obtained if the second neutron star receives a kick substantially smaller (velocity dispersion less than 50 km/s) than kick velocities commonly assumed for single radio pulsars. If this conclusion is correct, values of β_{ns} derived from simulations with low kick velocity dispersion are more likely and will be adopted here. Clearly, the natal kick amplitude remains the major source of uncertainty in the estimate of the fraction of bound NS-NS binaries. However, once the relative number of NS-NS binaries is fixed, the fraction f_b of massive binaries formed among all stars is related to β_{ns} through the equation

$$\frac{N_p}{N_b} = \frac{1}{\beta_{ns}} \frac{(1 - f_b)}{f_b} + 2 \frac{(1 - \beta_{ns})}{\beta_{ns}} \quad (2)$$

where N_p and N_b are respectively the number of single pulsars and the number of NS-NS binaries in the Galaxy. We have taken into account that the population of single pulsars results not only from the evolution of single stars but also partially from disrupted massive binaries. Since $f_b = 1$ is a strong upper limit, this imposes a lower limit for β_{ns} for a given ratio N_p/N_b . The number of isolated pulsars N_p has been derived from population synthesis of single radio pulsars. We have employed the code described in detail in Ref. 23, 24, up-graded to take into account the new pulsars discovered at high frequencies by the Parkes Multibeam Survey as well as the most recent model for the pulsar velocity distribution³⁰. The method consists

in generating population of pulsars with a given set of birth properties, following their evolution according to the dipole braking model and modeling selection effects that constrain radio detection. The best agreement between simulated and observed distributions of physical properties as the period, period derivative, distance, among others fixes the initial period and magnetic braking timescale distributions (see parameters in Table 1), as well as the total number of pulsars in the Galaxy ($N_p \approx 250000$) and their birthrate (one pulsar every 90 yr). Simulations using the recent results by Ref. 31 for the velocity distribution of radio pulsars were also performed and no significant differences in the values derived for parameters shown in Table 1 or for the total number of pulsars were noticed.

Table 1. parameters of the initial period P_0 and magnetic braking timescale $\ln \tau_0$ distribution, assumed to be Gaussian

| mean | dispersion |
|------------------------------|-------------------------------------|
| $P_0(ms) = 240 \pm 20$ | $\sigma_{P_0} = 80 \pm 20$ |
| $\ln \tau_0(s) = 11 \pm 0.5$ | $\sigma_{\ln \tau_0} = 3.6 \pm 0.2$ |

The number of NS-NS binaries can be derived by linking the properties of the youngest pulsar in a given double neutron star system, supposed not to have been affected by external torques, to those of the population of single pulsars. In other words, if the evolution of the newly formed (second) pulsar was not yet affected by torques other than the canonical magnetic dipole, its rotation period increases as those of isolated pulsars. For this set of simulations, we have adopted a velocity distribution for the barycenter of the NS-NS binaries different from the velocity distribution adopted for single pulsars. We consider that millisecond pulsars (MSP) were spun-up by mass transfer, before the second supernova explosion, which disrupted the system. According to Ref. 32 MSP have a Maxwellian velocity distribution, corresponding to a mean space velocity of 130 km/s. This velocity distribution must be that of those binary systems that survived the first supernova explosion³². Therefore, we have supposed that binary systems which have also survived to the second explosion have a velocity distribution similar to those which have survived to the first explosion. The mean transverse velocity of observed MSP is around 90 km/s, which corresponds exactly to the Maxwellian mean space velocity of 130 km/s derived by Ref. 29 from parametric likelihood analysis techniques. So far, two binary systems have been detected through the second pulsar: PSR B2303+46 and PSR J0737-3039 B. In order to observe two pulsars having millisecond like kick velocities, our simulations predict a total number of binaries $N_b = 730$, corresponding to a ratio $N_p/N_b = 342$. The advantage of our method is that we don't have to infer the statistical properties of binary pulsars from the very small observed sample and the only data we care about is the number of observed second born pulsars. The derived ratio N_p/N_b implies from Eq. (2), $f_b = 0.136$ if the value $\beta_{ns} = 0.024$ is adopted.

Notice that if the upper limit $f_b = 1$ is imposed to Eq. (2), then we conclude that $\beta_{ns} \geq 0.0058$ or that the 3-D velocity dispersion of the kick distribution of binaries should satisfy $\sigma < 270$ km/s, e.g., lower than that of the single population.

For each simulated NS-NS binary, the separation, the orbital period and the orbital eccentricity are available, allowing the calculation of the coalescence timescale τ due to emission of gravitational radiation. The cumulative number of pairs with a coalescence timescale less than τ varies as $N(< \tau) \propto \lg(\tau)$, corresponding to a probability distribution $P(\tau) = B/\tau$ (see Fig. 1) The simulations indicate a minimum coalescence timescale $\tau_0 = 2 \times 10^5$ yr and a considerable number of systems having coalescence timescales higher than the Hubble time. The normalized probability $P(\tau)$ in the range 2×10^5 up to 20 Gyr implies $B = 0.087$.

The other important term required for the evaluation of the coalescence rate from Eq.(1) is the star formation rate $R_*(t)$. In most of population synthesis models, in the absence of a detailed star formation theory, $R_*(t)$ is assumed to be proportional to the available mass of gas and under this (usual) assumption, from the mass-balance equation, it results $R_*(t) \propto e^{-\alpha t}$. In fact, we will use such an approach to model the evolution of an elliptical galaxy, as we shall see in the next section. In some even more simplified galactic models the star formation rate is assumed to be constant. However, for the Galaxy, the star formation history can presently be derived from observations and most of recent studies have inferred that the star formation activity is non-monotonic with time (Ref. 35 and references therein). Recent studies on the chromospheric activity index versus age relationship permitted the determination of ages for a sample of 552 stars from which was possible to reconstruct the star formation history of our Galaxy³⁵. These data indicate enhanced periods of star formation at 1 Gyr, 2-5 Gyr and 7-9 Gyr ago, probably associated with accretion and merger episodes from which the disk grows and acquires angu-

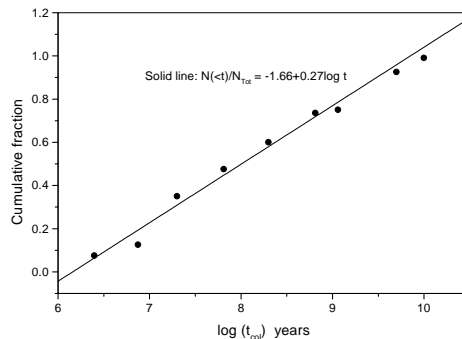


Fig. 1. The cumulative fraction of simulated NS-NS binary systems with coalescence time less or equal t . Time is given in years and the solid curve shows the best fit to the simulated data.

lar momentum²². Here we use the results by Ref. 35 to compute numerically the integral defined in Eq. (1). Using the numbers obtained, it results for the present galactic NS-NS coalescence rate $\nu_S = (1.7 \pm 1.0) \times 10^{-5} \text{ yr}^{-1}$. The estimated error is mostly due to uncertainties in the ratio N_p/N_b derived from simulations. Similar population synthesis calculations to estimate the birth-rate of compact binaries have also been performed by Ref. 36. However some differences exist between their and the present calculations. In the one hand, Ref. 36 normalized their birthrates to the type II+Ib/c supernova frequency, which was assumed to be constant over the lifetime of the galactic disk. Moreover, they have assumed that NS-NS binaries have the same natal kick distribution as that observed for single pulsars. On the other hand, our calculations took into account the star formation history of our Galaxy and the normalization was derived from two simulation sets, which fixed respectively the fraction of bound NS-NS pairs and the ratio between binary and single pulsars. However, it is worth mentioning that the cumulative number of NS-NS pairs with a coalescence timescale less than τ , resulting from both set of simulations is similar.

2.2. *The coalescence rate in ellipticals*

Excluding the Milk Way, no direct information is available for the neutron star population and the star formation history of other galaxies. Thus, the coalescence rate in extragalactic objects can only be estimated theoretically. In this case, we have assumed for elliptical galaxies the same values derived for the Milky Way for the parameters f_b, β_{ns} . It is worth mentioning that previous estimates of the present coalescent rate in ellipticals²⁰ lead to values which were about a half of that estimated for the Galaxy. However, in that work the star formation efficiency was constrained essentially by the present amount of gas in ellipticals, a very uncertainty quantity. A grid of models for elliptical galaxies was recently built in Ref. 37, including the effects of mass-loss by a galactic wind, responsible for the enrichment of the intra-cluster medium in metals. In these models, the parameters characterizing the star formation efficiency and the IMF were chosen by an iterative procedure in order to reproduce the color-magnitude diagram, (U-V) against M_V of ellipticals in Coma and Virgo clusters. We take their model 3 as a representative of a typical E-galaxy, defined by an initial mass equal to $2 \times 10^{11} M_\odot$ and a present luminosity $L_B = 2.9 \times 10^{10} L_{B,\odot}$. The IMF in these models are slightly flatter than the Salpeter's law ($\gamma \approx 2.19$) and the corresponding λ parameter is $\lambda = 8.71 \times 10^{-3} M_\odot^{-1}$. It should be emphasized that although the color-magnitude diagram imposes essentially constraints on low mass stars, the models also explain quite well the relative abundance of the α -elements, determined by massive stars, since they reproduce the observed metallicity indices like Mg_2 and $\langle Fe \rangle$ ³⁷. Under these conditions, the estimated present coalescence rate is $\nu_E = 8.6 \times 10^{-5} \text{ yr}^{-1}$. Notice that this value is about a factor of 5 *higher* than the galactic rate estimated in the previous section. Thus, in spite of fact that today ellipticals have practically a non-existent (or a very low) star formation activity, since the bulk of their stars were formed in the first 1-2

Gyr, the pairs merging today were copiously formed in the past with long coalescence timescales. A similar phenomenon occurs with type Ia supernovae. No type II supernovae are detected in ellipticals because these objects are the consequence of the evolution of massive stars, which have a rather short lifetime. However, type Ia supernovae are the only class detected in early type galaxies. This class of supernova is the consequence of the evolution of binary systems constituted by intermediate mass progenitors, which evolve into white dwarfs. The explosion of the compact object depends on the distribution of the merging timescale and only systems with long evolutionary timescales will explode by now.

In Fig. 2 we show the evolution of the merging rate for the Milky Way and for our representative model of an elliptical galaxy. The smoothness observed in the curve describing the evolution of the coalescence rate in the E galaxy is a consequence of the fact that the bulk of the stars are quite old, being formed in a short time interval. Since the probability to have a merger is inversely proportional to the time, the curve reflects essentially this fact. This is not the case for our Galaxy, since its disk is built gradually and the star formation rate may suddenly vary as new matter is accreted.

2.3. The local coalescence rate

The models developed by Ref. 37 can equally reproduce the colors of S0 galaxies. If we assume that the coalescence rate estimated above is typical for E and S0 galaxies having absolute magnitudes of about $M_B = -20.7$ and that the fraction of these objects is about 35%, then the weighted local coalescence rate can be written

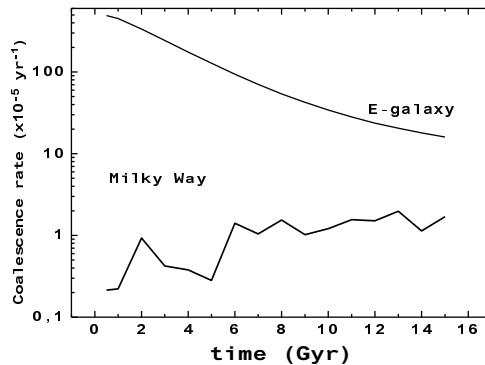


Fig. 2. Evolution of coalescence rates for the Milk Way and for a typical E galaxy. Notice that in the elliptical the bulk of stars is formed very early and the merging rate reflects mainly the probability of a NS-NS binary to coalesce in a given timescale. For the Galaxy, the star formation is continuous and intermittent, producing a modulation effect in the coalescence rate history

as

$$\nu_c = \nu_S(f_S + f_E \frac{\nu_E}{\nu_S} \frac{L_S}{L_E}) \quad (3)$$

where $f_S = 0.65$ and $f_E = 0.35$ are respectively the adopted fractions of spirals and (E+S0) galaxies, the ν_i 's and L_i 's are the respective coalescence rates and luminosities. From this relation and values obtained before, the local mean weighted coalescence rate is $\nu_c = 3.4 \times 10^{-5} \text{ yr}^{-1}$. In the one hand, had we usually assumed the local merger rate equal to the galactic one, neglecting the contribution of (E+S0) galaxies, we would have obtained a value smaller by a factor of two. On the other hand, the very recent galactic rate derived by Ref. 18 seems to overestimate by a factor of 2.5 our results for the total local rate, which include NS-NS mergers occurring in galaxies other than the Milky Way.

3. Expected detection rates

Extrapolation from the local coalescence rate to the expected rate within the volume $\frac{4\pi}{3} D^3$ is made multiplying the local value by the factor $K_B(< D)$, which is defined as the ratio between the *total* blue luminosity within the considered volume and the Milky Way luminosity ($L_{B,MW} \approx 2.3 \times 10^{10} L_\odot$). If galaxies were distributed homogeneously in the local universe, the scale factor correcting the local coalescence rate would simply be $K_B(< D) \approx 0.02 D_{Mpc}^3$. This approximation is probably reasonable for distances beyond 150 Mpc but underestimates the total luminosity in the B-band at lower distances, due to significant anisotropies in the distribution of galaxies. Moreover, the sensitivity of interferometric detectors is not isotropic, being larger to signals coming from above and below the plane. In this paper, the directional sensitivity of the detector and the anisotropy in the distribution of galaxies will not be taken into account as in Ref. 19. However, real counts of galaxies inside a given volume will be considered, allowing a more realistic evaluation of the total luminosity. Analyses of the spatial distribution of galaxies for $z < 0.033$ have been performed by Ref. 38 (and references therein) using the LEDA (Lyon-Meudon Extragalactic Database) catalog, which contains over one million of galaxies covering all-sky, including also a sub-sample of 134,000 objects having a measured redshift. The completeness of the catalog was evaluated by counts of galaxies up to a given magnitude, excluding galaxies in the zone of avoidance ($b < |15^\circ|$), which includes superclusters like the Great Attractor. According to Ref. 38, the redshift catalog is complete at level of 84% up to $B = 14.5$ and at a level of 90% for galaxies brighter than $B = 11.0$. It is worth mentioning that up to $B = 14.5$, the total luminosity does not increase as the cube of the distance, but more slowly with an exponent ~ 2.5 . Ref. 38 considered different volume limited samples, including only galaxies brighter than a given absolute magnitude. We correct for the absence of faint galaxies, supposing a Schechter luminosity function in the magnitude interval $-15 > M_B > -22$. Recent deep optical surveys in the zone of avoidance^{39,40,41} confirm the existence of a large structure dubbed the "Great Attractor" in the

region $|b| < 10^\circ$ and $316^\circ < l < 338^\circ$. This structure seems to be the intersection between the Centaurus Wall and the Norma supercluster, including some other clusters as the Centaurus-Crux complex. The center of the Great Attractor seems to be located at the Norma cluster (A3627) at $V_z = 4844$ km/s³⁹ and up to now 4423 galaxies have been identified as members of this supercluster. The total mass of such a complex is uncertain. A lower limit of $4 \times 10^{15} M_\odot$ is derived from direct counts and the observed velocity dispersion of the clusters, under the assumption of dynamical equilibrium. From large scale motions in this region, a mass as high as $5 \times 10^{16} M_\odot$ was obtained⁴². If we assume a more conservative value of about $10^{16} M_\odot$ for the total mass of the complex and a typical mass-to-luminosity ratio of $150 M_\odot/L_{B,\odot}$, then the Great Attractor alone would give a relative contribution to the total luminosity of $K_B \approx 2900$, at a distance of 70 Mpc. This contribution was added to the total luminosity derived from data for distances $D \geq 70$ Mpc. In Fig. 3, the calculated NS-NS coalescence rate ratio inside a volume of radius D , given by local rate times the factor $K_B(< D)$, is shown as a function of the distance D . Variations due to the Virgo cluster and the Great Attractor are indicated. Notice that rates corresponding to about one event per year can be obtained only if the detector can probe distances at least of the order of 90-100 Mpc.

The strength of a signal observed in a given detector is characterized by its signal-to-noise ratio S/N , which measures the signal amplitude in terms of the detector's noise characteristics. This quantity depends on the source power spectrum, the noise spectral density of the detector $S_n(\nu)$ in Hz^{-1} and the adopted method of data analysis. For merging NS-NS pairs, the optimum S/N ratio is obtained by the

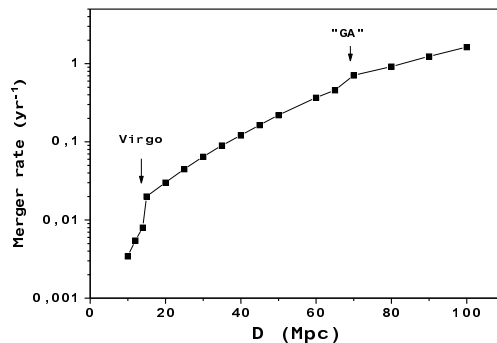


Fig. 3. Total expected NS-NS coalescence rate inside a volume of radius D as a function of D

so called matched filter, namely,

$$\left(\frac{S}{N}\right)^2 = 4 \int_0^\infty \frac{|\tilde{h}(\nu)|^2}{S_n(\nu)} d\nu \quad (4)$$

where $|\tilde{h}(\nu)|^2$ is the sum of the square of the Fourier transform of both polarization components. According to Ref. 43, the equation above can be written as

$$\frac{S}{N} = 8\Theta \left(\frac{r_0}{D}\right) \left(\frac{\mathcal{M}}{1.2M_\odot}\right)^{5/6} \zeta(\nu_{max}) \quad (5)$$

where D is the distance-luminosity to the source and the parameter r_0 is given by the relation

$$r_0 = 9.25 \times 10^{-22} \sqrt{I_{7/3}} \text{ Mpc} \quad (6)$$

with

$$I_{7/3} = \left(\frac{\nu_\odot}{\pi}\right)^{1/3} \int_0^\infty \frac{d\nu}{\nu^{7/3} S_n(\nu)} \quad (7)$$

where $\nu_\odot = 202.38$ kHz. The term $\zeta(\nu_{max})$ is defined by

$$\zeta(\nu_{max}) = \frac{(\nu_\odot/\pi)^{1/3}}{I_{7/3}} \int_0^{2\nu_{max}} \frac{d\nu}{\nu^{7/3} S_n(\nu)} \quad (8)$$

The spiral-in phase ends when the pair separation is such that tidal effects deform and may even disrupt the stars or when the last stable orbit is reached. In Eq. (8), $\nu_{max} \sim 750$ Hz corresponds to the maximum orbital frequency attained nearly the inner most circular orbit (see, for instance, Ref. 44). The other parameter appearing in Eq. (5) is the "chirp" mass $\mathcal{M} = \mu^{3/5} M^{2/5}$, with μ and M being respectively the reduced and the total mass of the system. The angular function Θ depends on geometrical projection factors of the detector, F_+ and F_X , for both polarization components (see, for instance, Ref. 45) and on the inclination between the orbital angular momentum of the binary and the line of sight, namely,

$$\Theta^2 = 4[F_+^2(1 + \cos^2 i)^2 + 4F_X^2 \cos^2 i] \quad (9)$$

The probability distribution of Θ was discussed in Ref. 46 and the authors have found an excellent approximation, which will be used here to estimate mean values

$$P(\Theta) = \frac{5\Theta(4-\Theta)^3}{256} \text{ if } 0 \leq \Theta \leq 4 \quad (10)$$

. From these equations, for a given S/N ratio and detector sensibility, the distance D probed by the instrument can be evaluated. For VIRGO and LIGO we have used the noise spectral density as given respectively by Refs. 47, 7 in a polynomial form, while for advanced-LIGO we have adopted the expression given by Ref. 48. Under these conditions, the parameter r_0 for each detector is 7.6 Mpc for VIRGO, 8.0 Mpc for LIGO and 120 Mpc for advanced-LIGO. Adopting $S/N = 7.0$, typical threshold for a false alarm rate of about one per year, the maximum probed distances are 13, 14 and 207 Mpc for VIRGO, LIGO and advanced-LIGO respectively. Using data

from Fig. 2, the mean expected event rates are one each 125 yr for LIGO, one each 148 yr for VIRGO and 6 events per yr for advanced-LIGO. In a recent study, Refs. 49, 50 have considered the spectral noise density of VIRGO in the context of chirp signal detection. Four main spectral regions were identified, according to the dominant source of noise: $\nu < 2$ Hz (seismic noise); $2 \text{ Hz} < \nu < 52$ Hz (pendulum thermal noise); $52 \text{ Hz} < \nu < 148$ Hz (mirror thermal noise) and above 148 Hz (shot noise). Rather than directing efforts to the lowest frequencies in the attempt to observe a large number of cycles, these analyses indicate that the reduction in the mirror thermal noise band provides the highest gain in the S/N ratio. The direct dependence of the mirror thermal noise power spectrum on the temperature suggests the use of already existing cryogenic techniques. In parallel, also the pendulum thermal and shot noises should be reduced in the mirror thermal noise band. If the total noise in such band could be reduced by a factor of 10, a gain by a factor of 8 can be obtained, increasing the maximum probed distance up to 100 Mpc for $S/N = 7$ and allowing an expected detection rate of about 3 events every two years. A recently proposed sound configuration⁵¹ for VIRGO would have a noise reduction through a large bandwidth and a similar expected detection rate. In this configuration the pendulum noise would be reduced by a factor of 8, the mirror thermal noise by a factor of 7 and the shot noise by a factor of 4. These results suggest that only the planned sensibility of the second generation of interferometers will permit to probe the local universe deep enough in order that at least few events should be seen in a monitoring period of one or two years. An alternative strategy for the present generation of laser beam interferometers is the search of these events by using a network of detectors, since for a given false-alarm rate, the detection threshold is lowered as the number of detectors increases^{52,53}. Data analysis of chirp signals detected by a network of detectors, in particular the one constituted by the two LIGO (Hanford and Livingston) and VIRGO, was recently considered by Ref. 54. They have estimated the increased detection sensitivity for this particular combination of detectors and for a false-alarm rate equal to one per year and a detection probability of 95%. Using the numbers of their Table III, we derived a maximum probed distance of 22 Mpc and an expected detection rate of about one event every 26 yrs.

4. Conclusions

In spite of the numerous investigations performed by different groups in the past years on the coalescence rate of NS-NS binaries in the Galaxy, the uncertainties are still quite large, due to several badly known aspects concerning the evolution of massive binaries. In this work we have adopted a new approach to tackle this problem, calculating the coalescence rate from the star formation history of the galaxy and from the probability per unit of time for a NS-NS system to merger in a timescale τ . In the case of the Galaxy, the star formation history was directly derived from observations, using the chromospheric activity index as an age estimator. The

data suggest that the star formation rate is intermittent, consistent with a picture in which the disk is gradually built by successive accretion episodes. Our numerical simulations on the evolution of massive binaries show that only 2.4% of the pairs remain bound after the second supernova explosion. Our simulations indicate also that the probability per unit of time for a NS-NS pair to coalesce in a timescale τ is $P(\tau) = B/\tau$, in agreement with the early estimate by Ref. 20 and the recent simulations by Ref. 36. Our approach indicate that the galactic coalescence rate is presently $(1.7 \pm 1.0) \times 10^{-5} \text{ yr}^{-1}$, a value which has remained more or less constant in the past 9 Gyr. Elliptical galaxies also contribute to the local mean coalescence rate. We have adopted as a typical E-galaxy a model from a grid able to reproduce the observed color-magnitude diagram of early-type galaxies in Virgo and Coma clusters. The star formation efficiency and the initial mass function, required to evaluate the fraction of formed massive stars, are fixed by fitting the photometric properties, whereas the fraction of formed massive binaries and the fraction of pairs which remain bound were taken to be equal to the galactic values. Under these conditions, the typical coalescence rate for an elliptical (or S0 galaxy) of absolute magnitude $M_B = -20.7$ is about $8.6 \times 10^{-5} \text{ yr}^{-1}$. Notice that this value is about a factor of five higher than the galactic rate. The local coalescence rate, derived from an appropriate average weighted by the relative luminosities and abundances, is $3.4 \times 10^{-5} \text{ yr}^{-1}$. The expected coalescence within a volume of radius D was estimated by scaling the local mean rate with respect to the ratio between the total luminosity in the considered volume and the luminosity of the Galaxy. Galaxy counts from the LEDA data base were used to estimate the total luminosity. We have used the completeness estimates made by Ref. 38 and the Schechter luminosity function to correct for the absence of faint galaxies. The contribution of the Great Attractor was included by assuming that the total mass of this structure is about $10^{16} M_\odot$ and that the mean mass-to-luminosity ratio is $150 M_\odot/L_{B,\odot}$. Our results indicate that a rate of about one event per year can only be obtained if detectors can probe distances at least of the order of 80 Mpc. This is not the case for the present generation of large laser beam interferometers, since from their planned sensibility, one event each 148 yr is expected for VIRGO whereas one event each 125 yr is expected for LIGO. These rates are modified when a network including three detectors (Hanford, Livingston and VIRGO) are considered, since in this case the expected rate corresponds to one event each 26 years. Recently proposed improved VIRGO configurations may significantly raise the expected detection rate up to 3 events every two years. For advanced-LIGO, 6 events per year are expected to be seen.

Acknowledgments

T.R. is grateful to B.S Sathyaprakash for useful discussions and the authors thanks the referee of this paper for his usefull comments. This research was partially supported by a PPARC (UK) post-doctoral research associateship to T.R. A.S. was

14 *J. A. de Freitas Pacheco, T. Regimbau, S. Vincent and A. Spallicci*

supported by the European Space Agency (G. Colombo Senior Research Fellowship).

References

1. C. Bradaschia et al., *Nucl.Instrum.Meth. A* **289**, 518 (1990).
2. A. Abramovici et al., *Science* **256**, 325 (1992).
3. J. Hough, in *Proc. 6th Marcel Grossmann Meeting*, eds. H. Sato and T. Nakamura (World Scientific Singapore, 1992), p. 192
4. K. Kuroda et al., in *Proc. Int. Conf. on Gravitational Waves: Sources and Detectors*, eds. I. Ciufolini and F. Fiducaro, (World Scientific Singapore, 1997), p. 1007
5. J.A. Faber and F.A. Rasio, 2000, *PRD* **62**, 064012 (2000).
6. S. Rosswog, M.B. Davies, F.-K. Thielemann and T. Piran, *A&A* **360**, 171 (2000).
7. T. Damour, B.R. Iyer, B.S. Sathyaprakash, *PRD* **63**, 044023 (2001).
8. S.F. Portegies Zwart and H.N. Spreeuw, *A&A* **312**, 670 (1996).
9. S.F. Portegies Zwart and L. Yungelson, *A&A* **332**, 173 (1998).
10. K. Belczyński, V. Kalogera and T. Bulik, *ApJ* **572**, 407 (2002).
11. E.S. Phinney, 1991, *ApJ* **380**, L17 (1991).
12. E.P.J. van den Heuvel and Lorimer D., *MNRAS* **283**, L37 (1996).
13. V. Kalogera, R. Narayan, D.N. Spergel and J.H. Taylor, *ApJ* **556**, 340 (2001).
14. C. Kim, V. Kalogera and D.R. Lorimer, *ApJ* **584**, 985 (2003).
15. V. Kalogera et al., *ApJ* **601**, L179 (2002).
16. A.V. Tutukov and L.R. Yungelson, *MNRAS* **260**, 675 (1993).
17. V.M. Lipunov, K.A. Postnov and M.E. Prokhorov, *MNRAS* **288**, 245 (1977).
18. V. Kalogera et al., *ApJ* **614**, L137 (2004).
19. P. Nutzman et al., *ApJ* **612**, 364 (2004).
20. J.A. de Freitas Pacheco, *Astrop. Phys.* **8**, 21 (1997).
21. A. Helmi, S.D.M. White and V. Springel, *MNRAS* **339**, 834 (2003).
22. S. Peirani, R. Mohayaee and J.A. de Freitas Pacheco, *MNRAS* **348**, 921 (2004).
23. T. Regimbau J.A. and de Freitas Pacheco, *A&A* **359**, 242 (2000).
24. T. Regimbau J.A. and de Freitas Pacheco, *A&A* **374**, 182 (2001).
25. S. Vincent, 2002, DEA Dissertation, University of Nice-Sophia Antipolis, France
26. V. Trimble, *AJ* **79**, 967 (1974).
27. Z.T. Kraicheva, E.I. Popova, A.V. Tutukov and L.R. Yungelson, *AZh* **55**, 1176 (1978).
28. J. D. M. Dewi, Ph. Podsiadlowski and O. R. Pols, *MNRAS*, to be published, astro-ph/0507638
29. J.M. Cordes and D.F. Chernoff, *ApJ* **482**, 971 (1997).
30. Z. Arzoumanian, D.F. Chernoff and J.M. Cordes, *ApJ* **568**, 289 (2002).
31. Hobbs et al., *MNRAS*, **360**, 974 (2005).
32. A. G. Lyne, R. N. Manchester, D. R. Lorimer, M. Bailes, N. D'Amico, T. M. Tauris, S. Johnston, J. F. Bell, L. Nicastro, *MNRAS* **295** (1998).
33. T.M. Tauris, M. Bailes, *A&A* **315**, 432 (1996).
34. A. G. Lyne, F. Graham-Smith, *Pulsar Astronomy*, (Cambridge University Press, Cambridge, 1998)
35. H.J. Rocha-Pinto, J. Scalo, W.J. Maciel and C. Flynn, *ApJ* **531**, L115 (2000).
36. R. Schneider, V. Ferrari, S. Matarrese and S.F. Portegies Zwart, *MNRAS*, **324**, 797 (2001).
37. T.P. Idiart, R. Michard and J.A. de Freitas Pacheco, *A&A* **398**, 949 (2003).
38. H. Courtois, G. Paturol, T. Sousbie and F.S. Labini, *A&A* **423**, 27 (2004).
39. R.C. Kraan-Korteweg, *LNP* **556**, 301 (2000).

40. P.A. Woudt and R.C. Kraan-Korteweg, Mapping the Hidden Universe: The Universe behind the Milky Way - The Universe in HI. *Proc. Conf. APS*, eds. R.C. Kraan-Korteweg, P.A. Henning, and H. Andernach (Astronomical Society of the Pacific, 2000), Vol. 218, p. 193
41. P.A. Woudt and R.C. Kraan-Korteweg, *A&A* **380**, 441 (2001).
42. D. Burstein, *Rep.Pro.Phys.* **553**, 421 (1990).
43. L.S. Finn, *PRD* **53**, 2878 (1996).
44. E.E. Flanagan and S.A. Hughes, *PRD* **57**, 4535 (1998).
45. P. Jaranowski, A. Królak and B.F. Schultz, *PRD* **58**, 063001 (1998).
46. L.S. Finn and D.F. Chernoff, *PRD* **47**, 2198 (1993).
47. M. Punturo, VIR-NOT-PER-1390-51 (2003).
48. B.J. Owen et al., *PRD* **58**, 084020 (1998).
49. A. Spallicci, VIR-NOT-OCA-1390-257 (2003).
50. A. Spallicci, S. Aoudia, J.A. de Freitas Pacheco, T. Regimbau and G. Frossati, to appear in *Class. Quantum. Grav.*, **22**, 461 (2005).
51. M. Punturo, VIR-NOT-PER-1390-283 (2004).
52. B.F. Schultz and M. Tinto, *MNRAS* **224**, 131 (1987).
53. N. Arnaud et al., VIR-NOT-LAL-1390-165 (2001).
54. A. Pai, S. Dhurandhar and S. Bose, 2002, *PRD* **64**, 042004 (2002).